

Materials and Manufacturing Methods for EWOD Devices: Current Status and Sustainability Challenges

Oriol Caro-Pérez,* Jasmina Casals-Terré, and Maria Blanca Roncero


Electrowetting-on-dielectric (EWOD) devices have proven to be effective tools for precise microfluidic manipulation or in liquid lenses that surpass conventional solid lenses in versatility. However, the fabrication of these devices presents many challenges, such as their scalability or the growing concern on their environmental impact due to materials used in their fabrication. This review provides a comprehensive analysis of the materials currently used in the fabrication of EWOD devices and the characteristics they must meet. In addition, a discussion of future challenges in the fabrication of EWOD devices is presented, in particular the environmental problems presented by some of the materials currently in use.

1. Introduction

The handling of small-volume for nanometer-scale liquids is one of the biggest challenges in the analytical industry today. Microfluidics is the science and technology that offers an optimal solution to these challenges. Among the solutions offered by microfluidics, digital microfluidics (DMF) has gained great interest in recent years (Figure 1). DMF is a single drop handling-based technology that uses electrowetting-on-dielectric (EWOD) effect to manipulate fluids without the need for complex microfluidic channels. The EWOD effect explains the decrease in the contact angle (CA) of an ionic liquid that is subjected to an electrical voltage. Its simplicity lies in its pump-less or valve-less operation. Its strengths include the ability to manipulate fluid just without the need of external pressure sources and its wide range of lab-on-chip applications.

O. Caro-Pérez, M. B. Roncero
 CELBIOTECH_Paper Engineering Research Group
 Universitat Politècnica de Catalunya BarcelonaTech (UPC)
 Colom Street 11, Terrassa 08222, Spain
 E-mail: oriol.caro.perez@upc.edu

J. Casals-Terré
 Department of Mechanical Engineering
 Universitat Politècnica de Catalunya (UPC)
 MicroTech Lab, Colom Street 11, Terrassa 08222, Spain

 The ORCID identification number(s) for the author(s) of this article can be found under <https://doi.org/10.1002/mame.202200193>

© 2022 The Authors. Macromolecular Materials and Engineering published by Wiley-VCH GmbH. This is an open access article under the terms of the Creative Commons Attribution License, which permits use, distribution and reproduction in any medium, provided the original work is properly cited.

DOI: 10.1002/mame.202200193

The origin of the EWOD use goes back to Lippmann in 1875, with the first studies on electrocapillarity using mercury and other conductive liquids.^[1] Later, when electrowetting (EW) investigations focused on the behavior of ionic liquids on metal directly, A. Frumkin described, the changes in the CA of the ionic liquids subjected to a voltage on a metal surface.^[2] However, the studies were more focused on the electrochemistry than on the EW effect. It was not until 1981 that Beni^[3] named the phenomenon electrowetting as the basis for a display device that could change from being transparent to white (diffusely reflecting) as a result of a change in the behavior of a

liquid inside a capillar when an electric voltage was applied. But the EWOD implementation for liquid handling was not possible until the incorporation of dielectric layers in 1993 with the studies of Berge,^[4] renamed as electrowetting-on-dielectric.

Initially, the use of this phenomenon was focused on the field of liquid optics,^[5] DMF, and lab-on-chip^[6,7] applications. However, novel functionalities such as self-cleaning surfaces^[8,9] or surface functionalization^[10] have recently been proposed. On lab-on-chip applications, EWOD devices have the advantage over the other microfluidics devices to allow handling of small volumes individually. This technique dilutes without dead-volume losses compared to other techniques that have important dead-volumes such as paper-based microfluidic or conventional capillary driven-microfluidics. This advantage is critical, as the number of analytes to be analyzed has increased in clinical practice, but the sample size remains the same. It is also compatible with automation trends in clinical analytical practice. In optical applications, EWOD devices are able to change the lens focal length without adding other lenses or complex mechanical parts.

EWOD devices present three main functional layers: the conductive layer, the dielectric layer, which insulates the electric current of the ionic liquid, and the hydrophobic layer, which reduces the surface energy to a minimum.

The conductive layer can be made out of a wide range of materials. Even though, most of the studies focus on the electrode gap reduction^[7,11,12] and the electrode geometry,^[13–15] more than in the material itself. The studies on electrode geometry aim to facilitate the speed of droplet manipulation^[16,17] or the easiness of the droplet transfer directions,^[12] to enable the droplet splitting/joining or to perform dilutions or concentrations of a solution.^[18,19]

On the other hand, the study of the dielectric layer pursues the understanding of the effects of its thickness, the dielectric

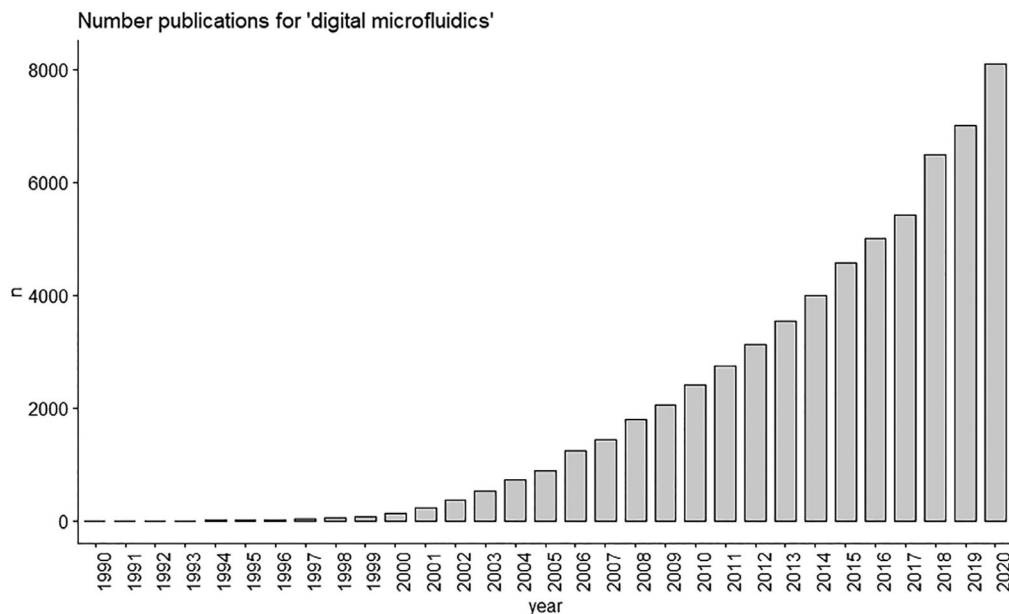


Figure 1. Exponential rise in the number of EWOD studies. Results from Google Academics for “digital microfluidics.”

constant and the breakdown field^[20,21] on the EWOD phenomena. The objective is to achieve a lower actuation voltage,^[22] a lower CA, an understanding of the saturation phenomenon,^[23–26] and/or the search for different materials, which can provide more flexibility on the kind of fabrication processes used.

Another fact to consider is that these devices must have a very high CA in order to reduce surface adhesion, therefore materials with low surface energy are required.^[22] Currently, most designs use fluoride materials, which produce a high environmental impact at the end of their life cycle. Novel strategies are incorporated to improve CA without the use of harmful materials such as biomimetic surface structuring following the lotus effect.^[23]

The following review will provide an overview of the requirements of an EWOD device, starting from a number of studies which explain in a simple way the theoretical background of the EWOD effect. This overview is necessary to address the issues that are arising when transferring this technology to the everyday use. An overall picture of current trends is presented by analyzing the manufacturing methods and the driving voltages required of devices in state-of-art papers. This includes an analysis of the novel materials and manufacturing processes that have appeared and can help to meet the growing trends and needs in our society, such as lowering the social environmental impact. The use of biodegradable materials or the ability for on-site manufacturing should be important features to be considered when design new EWOD devices.

2. EWOD Theory

The behavior of a droplet on a surface was first described by Thomas Young^[27] Thomas reported that a droplet resting on a solid surface forms, a characteristic CA on this surface (θ_0). The cosines of this CA can be calculated from the relationship be-

tween the free energy of the liquid-fluid (γ_{lf}), solid-liquid (γ_{sl}), solid-liquid (γ_{sl}), and solid-fluid (γ_{sf}) interfaces as

$$\cos \theta_0 \gamma_{lf} = \gamma_{sf} - \gamma_{sl} \quad (1)$$

Thus, we understand a hydrophilic surface as one that has a γ_{sl} smaller than γ_{sf} , with a positive cosine, which means a CA of less than 90° . When, γ_{sl} is greater than γ_{sf} , the cosine will be negative, therefore, the CA is greater than 90° . This relationship is always applicable to a perfectly smooth^[28] and chemically homogenous surface.^[29]

A liquid's behavior on a solid surface can be explained by the spreading parameter (S)

$$S = \gamma_{sf} - (\gamma_{lf} + \gamma_{sl}) \quad (2)$$

if S is positive, then the wetting is complete. Otherwise, if S is negative, the wetting is partial, and the droplet remains on the surface.

When a drop hits a solid surface, the liquid expands across the surface up to a maximum diameter. At this point, two forces are present that counteract each other until an equilibrium. The ratio of these two forces is called the capillary number. The capillary number is a dimensionless value representing the ratio between the viscous force of a liquid and the surface tension force:^[30]

$$Ca = \frac{\sigma R}{\gamma_{LF}} = \frac{\eta \dot{\gamma}_{LF}}{\gamma_{LF}/R} \quad (3)$$

where R is the radius of the drop, γ_{LF} is the liquid-fluid interfacial tension, and η is the viscosity of the liquid. Upon impact, the kinetic energy of the droplet is transformed into surface energy, spreading the liquid on the surface. The surface tension (γ_{LF}/R) retracts the liquid to form the droplet again, while the viscous

force of the liquid ($\sigma = \eta\gamma_{LF}$) dissipates it. When $Ca > 1$, the surface forces prevail the viscous forces. When $Ca < 1$, surface forces are predominant over viscous forces.

However, real surfaces present irregularities that can be either due to the chemistry of the surface or the roughness of the surface. For instance, chemical modifications change the surface energy of the surface.^[31] These surface irregularities cause differences between the observed and the predicted CA as well as an increase in the hysteresis, which causes a different forward and backward CA.

The surface roughness size has a great influence on the CA of a liquid on a surface. In a large roughness surface, the forward and backward angles of a droplet's hysteresis are well captured by Equation (1).^[32] However, this is not true, in small roughness surfaces ($< 1 \mu\text{m}$). In this case, the droplet rests at its minimal free energy, with a CA different from the one predicted by Young (Equation (1)). Wenzel introduced the roughness factor in its equation and according to him,^[33] the CA could be explained as

$$\cos \theta_w = r \frac{\gamma_{sf} - \gamma_{sl}}{\gamma_{lf}} = r \cos \theta_0 \quad (4)$$

where r is the roughness factor and θ_w is the Wenzel CA. This r is the ratio between the actual contact area and the area projected by the droplet.

Therefore, for a perfectly smooth surface, $r = 1$, while on a rough surface, $r > 1$. Under this situation, a surface that is hydrophilic becomes more hydrophilic. While, a surface that is hydrophobic becomes more hydrophobic.

In a simplified model, where the roughness is made up of regular columns,^[34,35] r can be calculated with following formula^[35]

$$r = \frac{G + W + 2H}{G + W} \quad (5)$$

where G is the pore size, H is the pore depth, and W is the pore spacing (Figure 2).

To explain the CA in the case of a rough surface where air is trapped between the liquid and the surface, in 1944, Cassie and Baxter^[36,37] studies assumed that the rough surface was composed of air pockets and the solid. The Cassie Baxter CA was calculated as the sum of the cosines of the CA generated by the liquid on the two material, weighted by the amount of available surface. If one of the surfaces is just air, the cosine of the CA on this surface is -1 , leading to the following equation

$$\cos \theta_{CB} = r (\cos \theta_0 + 1) - 1 \quad (6)$$

where θ_{CB} is the apparent CA in Cassie-Baxter state and r is a roughness factor. If r decreases, the less CA there is between the droplet and the surface due to the trapped air.

The Cassie-Baxter and Wenzel effects can be observed on different areas of the same surface, depending on how the droplet is formed.^[38] When a drop falls on a rough surface, either of these two states can occur, as long as, the energy of the surface roughness is less than the capillary force^[39]. To go from a Cassie-Baxter to Wenzel state, there is an energy barrier, the Wenzel effect being understood as a state of minimum energy.^[40]

In the electrowetting effect, an ionic liquid is subjected to an electric potential. A layer of ions with a charge opposite to the

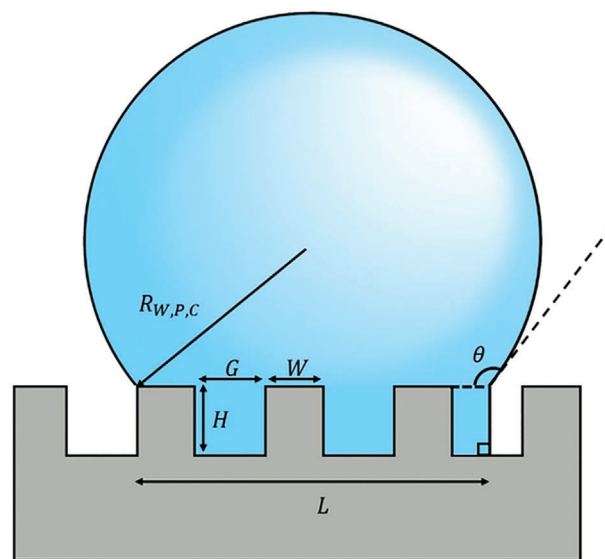


Figure 2. The different variables present on a rough surface that modify the contact angle presented by a drop. Reproduced with permission under the terms of the CC-BY license.^[35] Copyright 2016, the Authors. Published by Springer Nature.

electric potential accumulates at the solid-liquid interface. This layer is referred as the electric double layer.^[41-43] The resulting electrostatic force pulls this layer towards the outside part of the droplet, causing a decrease in the CA at the three-phase interface or triline.^[41] A dielectric layer prevents the contact of the liquid volume with the two electrodes, avoiding a short circuit and the electrolysis of the liquid.^[44]

The behavior of an EWOD device is described by a capacitor with a distributed electrostatic potential when the system is charged.^[45] This charge distribution changes the initial CA between the liquid and the surface defined by the Lippmann-Young equation (Equation (1)).^[46] Therefore, the resulting Lippmann-Young equation that relates the change of the CA to the applied voltage field and the material properties is

$$\cos \theta_v - \cos \theta_0 = \frac{C}{2\gamma} V^2 \quad (7)$$

where θ_v and θ_0 are the CA under the electric field and without the applied electric field, respectively. The capacitance is represented by C , γ is the surface tension of the liquid, and V is the voltage due to the applied electric field.

Capacitance is the difference between the magnitude of the charge on one of the conductors and the potential difference between them

$$C = \epsilon_0 \epsilon_d \epsilon_h \frac{A}{\epsilon_d t_d + \epsilon_h t_h} \quad (8)$$

where ϵ is the dielectric constant and t is the thickness of the layer, differentiated by the subscripts 0, d , and h corresponding to the free space, the dielectric layer, and the hydrophobic layer, respectively. The area projected by the electrode is A .

The potential energy accumulated on the droplet can cause the shift between the Cassie-Baxter energy state and the Wenzel

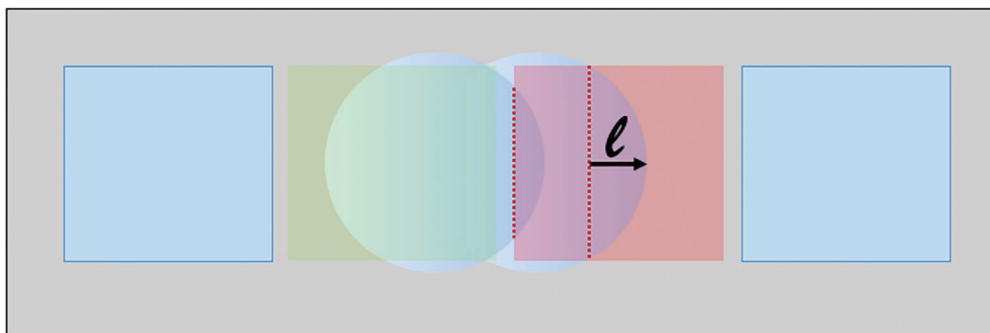


Figure 3. The effective contact line length (red dashed line) increases with droplet displacement.

energy state. Once this energy barrier is overcome, the new irreversible state of minimum energy is the Wenzel energy state.^[47]

Even though the formula forecasts a voltage for the complete wetting ($\theta_v = 0$), experimentally, it is not possible to reach this value, since there will not be further change in the CA. This phenomenon is known as CA saturation,^[19] which is still under study.^[48,49]

In certain configurations, the movement of an EWOD-driven droplet can be achieved by the unbalance of the electrostatic forces, the surface tension forces and/or the hydrostatic pressures in the front part and rear part of the droplet.^[50] The electrostatic force causes a decrease of the CA on the side of the droplet that is in contact with the connected electrode.^[51] Since the size of the electrode is larger than the fraction of the droplet laying on it, this electrostatic force pulls the droplet towards the part of the electrode that is not covered by the liquid.

The motion is achieved due to the unbalance of forces between an active and a nonactive electrode. The capillary force applied at the triple line (f_w), which is the interface between the droplet, the surface and the substance surrounding the droplet, is defined as

$$f_w = \gamma_{lf} (\cos\theta_v - \cos\theta_0) \quad (9)$$

where f_w is the capillary force, γ_{lf} is the free energy liquid-fluid, θ_v and θ_0 are the CA under the electric field and without the applied electric field, respectively.

Performing the integral, we can obtain the vector force (F_x) in the direction of motion, which is expressed as

$$F_x = L\gamma_{lf} (\cos\theta_v - \cos\theta_0) \quad (10)$$

Substituting Equation (7) into Equation (4), the force required to generate the EWOD effect is obtained. This force can also be expressed in terms of the voltage and the material properties, when the two electrodes are considered a parallel plate capacitor

$$F_x = \frac{1}{2} \frac{\epsilon_f \epsilon_r L}{d} V^2 \quad (11)$$

where L is the effective length of the contact line (red dashed line in **Figure 3**). The length of the contact line (L) is determined by the formation of the boundary structure of the adjacent electrode (**Figure 3**), d is the distance between electrodes, ϵ_r is the dielectric constant, and ϵ_f is the free space permittivity.

Finally, the driving force moving the droplet can also be expressed as a pressure gradient within the body of the ionic liquid itself, with the lower pressure side corresponding to the fraction of the droplet on the active electrode by EWOD. The formula defining this force is as follows:

$$F_e = (P_t - P_a(v)) h \quad (12)$$

where P_t is the hydrostatic pressure in the non-EWOD actuated part of the droplet, $P_a(v)$ is the hydrostatic pressure in the EWOD actuated part of the droplet, and h is height difference between the top of the nonactuated droplet and the EWOD actuated part of the droplet.

The sum of the electrostatic forces (Equation (11)) and hydrostatic pressure (Equation (12)) would provide the total electromotive force of the device. However, there are forces that oppose the motion. In terms of friction force (F_f), this is determined by the normal force of the droplet (**Figure 4**) and the friction constant of the device:

$$F_f = \mu F_N \quad (13)$$

where F_N is the droplet normal force and μ is the coefficient of surface friction. In a recent paper,^[52] it has been shown that the friction force is directly proportional to the normal component of the surface tension. As a result, Amontons' first and second laws of rigid body friction are analogous to the F_N of a droplet. The value of friction has been replaced by the normal force of the vertical component of the contact angle

$$F_N = \pi w \gamma_{lf} \sin(\theta_e) \quad (14)$$

where π is the value of pi, w is the droplet diameter, and θ_e is the contact angle at saturation.

The coefficient of friction is defined as

$$\mu = \frac{k(\theta_F - \theta_B)}{\pi} \quad (15)$$

where k is a dimensionless shape factor for the three-phase contact line, θ_B is the back contact angle, and θ_F is the front contact angle of the droplet.

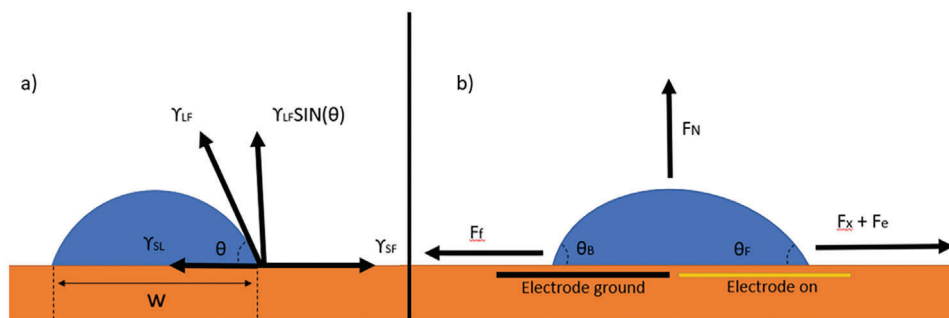


Figure 4. a) Components of the contact angle. b) Forces involved in droplet displacement on the surface of an EWOD device.

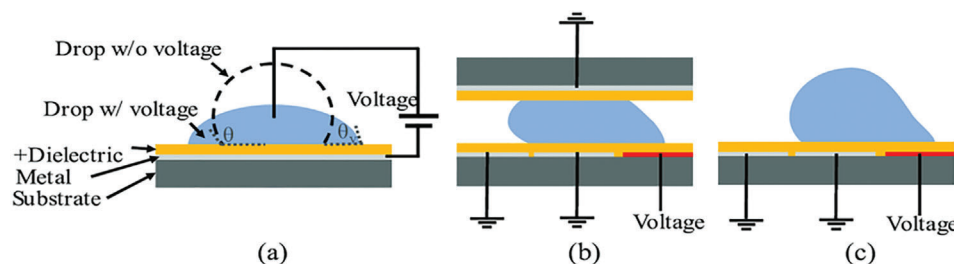


Figure 5. Different prototypes of EWOD devices. a) Conventional EWOD device, where the electrode drives the electrical voltage from the top of the droplet while on the surface, under a thin dielectric layer, is the grounded electrode. b) EWOD coplanar device with parallel plate, where the drive electrode is on the surface behind the dielectric layer and the grounded electrode is a plate on top. c) Single-plate coplanar EWOD device, where drive electrode and grounded electrode are located on the surface of the device behind the dielectric layer. Reproduced under the terms of the CC-BY license.^[27] Copyright 2019, the Authors. Published by MDPI.

3. Types EWOD Configurations

The EWOD devices have three main configurations: conventional (Figure 5a), parallel-plate coplanar (Figure 5b), and single-plate coplanar (Figure 5c).

The different configurations are applied according to the need and/or the application of the device. In applications where no motion is required, conventional EWOD devices are used. Such as the Fresnel lens combining several EWOD-driven liquid lenses designed by Enrico et al.^[53] or the combination of different optical lenses that could be actuated independently and modulate the light accurately allowing a precise change of the focal length.

Coplanar EWOD devices are specially designed for the dynamic handling of droplets on their surface. There are two types of coplanar EWOD devices: open-plate or single-plate (Figure 5c) and closed-plate or parallel-plate (Figure 5b) devices.

The most common EWOD device design is parallel-plate, in which a bottom plate contains directional electrodes and the top plate has a single grounded electrode. This configuration allows precise volume control.^[45] Moreover, this type of electrode is mostly used for droplet transport, droplet splitting and/or droplet fusion.^[54]

There is another version of the parallel-plate EWOD devices, which incorporates a conductive wire instead of a full plate on the top (Figure 6). This disables the fusion or fission of droplets. Moreover, since two surfaces are in contact with the droplet, therefore the adhesion forces are higher and the handling speed is lower. In this case, the minimum driving voltage of the EWOD device is higher than in the open configuration.^[55,56]

In the open configuration, both electrodes are on a single surface. This fact allows a more efficient use of the voltage and a higher droplet velocity. Because the fluid is only in contact with one of the surfaces and the adhesion and the dragging forces are lower.^[54,57]

4. EWOD Materials

In general, EWOD devices are made out of four functional layers: the substrate, the conductive layer, the dielectric layer, and the hydrophobic layer. Depending on the final application of the device, each layer must meet certain characteristics.

4.1. Substrates

The substrate mainly supports the functional layers of the EWOD device. In addition, it must be compatible with the purpose of the device. In an EWOD device that is designed for optical purposes, the substrate must be transparent. Li et al.^[58] designed an EWOD device coating the electrodes on a glass. This device has the ability to move and split an aqueous droplet. Another work that built the EWOD device on glass was designed by Högnadóttir et al. for the purpose of condensing moisture on its surface.^[59]

Besides transparency, another characteristic that is some time pursued by EWOD designers is flexibility. For instance, Cao et al. designed an EWOD flexible parallel-plate device with polytetrafluoroethylene.^[60] The possibility to build flexible and

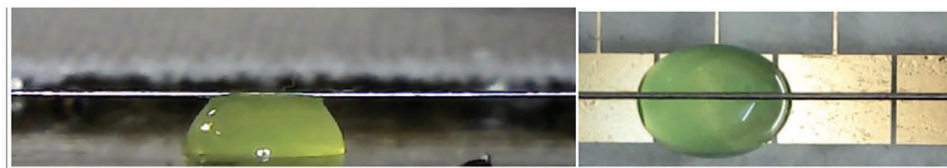


Figure 6. Parallel-plate EWOD with wire. Reproduced with permission^[55] Copyright 2022, Elsevier.

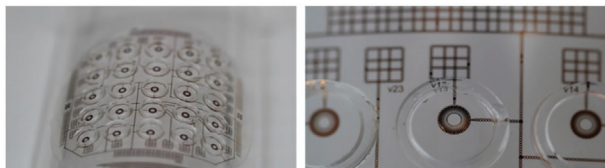


Figure 7. 5×5 matrix EWOD flexible and transparent device. At each point of the matrix, a liquid lens capable of focusing individually is obtained. Reproduced under the terms of the CC-BY license.^[62] Copyright 2019, the Authors. Published by MDPI.

transparent devices created novel applications such as: a self-cleaning surface^[61] and focus-tunable micro arrays of lenses with adjustable focus through voltage^[62] (see **Figure 7**).

When no transparency nor flexibility is required, the most common substrate materials are either the printed circuit board (PCB) or glass. These two common materials are readily available and have been widely used, but their current production methodology is not sustainable. Nowadays, it is intended to resort to the use of biodegradable materials to contribute to the sustainability and protection of the environment. The use of paper, a fully biodegradable material, is considered an alternative to provide flexible behavior when pressure is applied. In year 2019, Mogi et al. designed a paper-based EWOD device^[63] on paper.

The purpose of the device may limit the materials available to build the device. A flexible substrate has the ability to adapt its shape to the surface. However, it has the disadvantage that in the actuation of the device, a deformation of the soft substrate occurs on the triple contact line. This deformation on a microscopic scale is a consequence of the vertical force component occurring at the triple line of the droplet. This is known as a wetting ridge.^[64] This wetting ridge moves along with the triple droplet line on the surface.^[65] The presence of this wetting ridge dissipates the electromotive force of the device on the droplet.^[65] This means that EWOD devices with flexible substrates are less efficient and have a higher saturation angle. Another limitation that some materials may have due to their nature is roughness. In fact, the use of paper as a substrate is interesting because of its low environmental impact compared to the most commonly used materials, but it has a higher roughness. This implies a significant increase in the friction constant, which is linked to the friction force that opposes the electromotive force of the device.

4.2. Electrodes

4.2.1. Materials

The material used to create the electrodes does not depend on the final purpose of the device. However, the manufacturing technol-

ogy and the substrate nature limit the options of materials to be used.

Certain deposition methods require the use of specific equipment. Nampootheri et al. designed a cooling EWOD-based device^[14] and its electrodes were made out of chromium and gold by sputtering deposition. Basu et al. used thermal vapor deposition to build aluminum electrodes.^[66] These methods allow precise and high-resolution electrodes; however, the equipment is normally placed in environment controlled clean rooms, not always available for all designers.

EWOD devices offer the possibility to create highly accurate point-of-care device, which are of particular interest in country where public health system suffers from chronic burden. However, if their manufacturing process is complex, the adoption of this technology in growing economies is limited.

Places with limited resources or difficult access, such as disaster areas or during a pandemic, would benefit from other manufacturing methods. Joshi et al. in 2020 used inkjet printing to define silver electrodes for their EWOD devices.^[16] In another work, Mog et al. 2020,^[63] in which an EWOD device was designed on paper substrate, the electrodes were printed by a conventional inkjet printer using conductive ink.

Beyond the manufacturing methods, recent works have focused on the introduction of novel materials with interesting properties. For instance, Palma et al. in 2018 designed an EWOD device that uses conductive crystalline silicon.^[67] The use of this material allows an electric current to be induced using a light pulse.

4.2.2. Geometry

The geometry or shape of the electrode is a critical point in the design of the coplanar EWOD device. Shape and electrode gap influence on the droplet velocity, its directionality, and the capacity to split or merge the droplet.

Jain et al. studied electrode geometries and electrode spacing with a parallel-plate copper electrode EWOD device.^[55,68] **Figure 8** presents the four geometries studied: square, interdigitated, zigzag, and zigzag flat-base. The gap size ranged from 80 to 110 μm . The 80 μm gap electrode with zigzag flat-based geometry was the most efficient. According to Equation (11), the length of the contact line L (**Figure 3**) is directly proportional to the actuating force of the device. In addition, this geometry enables four possible directions of motion.

In similar way, Wang et al. presented an asymmetrical, heart-shaped design.^[16] This geometry causes a longer contact length of the droplet with the next electrode, which enhances the driving force. However, the droplet can only move in one direction. **Figure 9** shows the Basu et al. triangular electrode design.^[66] Even

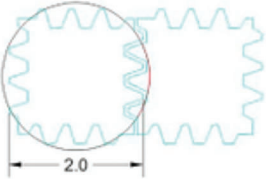
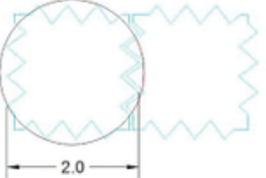
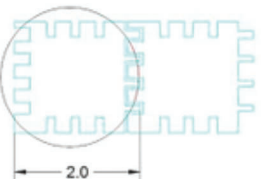
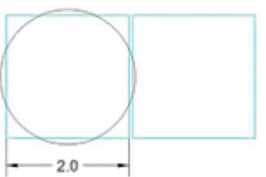
Electrode patterns	Electrode Gap(80 μm)	Contact line length (μm)
Zigzag-flat		1856
Zigzag		1612
Interdigitated		1428
Square		1387

Figure 8. Geometries with their corresponding contact line lengths in the study by Jain et al. Reproduced with permission.^[55] Copyright 2017, Elsevier.

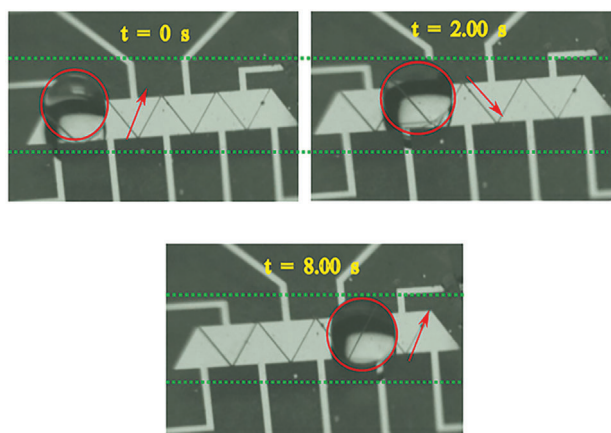


Figure 9. Experimental images of the triangular electrode design by Basu et al. Reproduced with permission.^[66] Copyright 2020, Elsevier.

though this geometry is not as efficient as Wang design, in terms of force generated, it allows a bidirectional droplet movement.

Zhang et al. chose a honeycomb design. This design allows the movement of a droplet in eight different directions.^[69] Another advantage of using a honeycomb design is that fewer drive electrodes are required, 7, compared to other designs, 9 in the square or 12 in the triangular design (Figure 10). However, as each side has a straight profile, the speed is lower than in zig-zag profiles.

Electrode geometry is not the only factor that defines speed or directionality. Wang et al. designed electrodes with different sizes (five) in their EWOD device.^[70] Therefore, they performed up to 49 different dilutions with their device.

Using a similar approach, Lejard-Malki et al. presented an EWOD device able to concentrate the sample' parasites.^[71] The authors optimized different electrode shapes in order to remove part of the droplet volume without loss of parasites, decreasing the initial volume from 10 microliters down to few nanoliters. The creation of vortices during the displacement of the droplet prevented the deposition of the parasites on the surface of the device.

Högnadóttir et al. took advantage of asymmetrically shaped electrodes to achieve moisture condensation into increasingly larger droplets.^[59] In this way, the device could be used as a self-cleaning surface or to capture moisture from the environment (Figure 11).

The critical issues of these designs are that they are limited to the application that they are thought for. Guan et al presented a design with n -electrodes that can be connected at the same time, generating a metaelectrode.^[12] The size of this metaelectrode is dependent on the total number of active electrodes (Figure 12). It additionally allows the electrode drop to move from strip to strip, achieving a more fluid displacement on the surface. The design of this device has made it possible to compare the droplet displacement velocity of rectangular electrodes versus square electrodes.

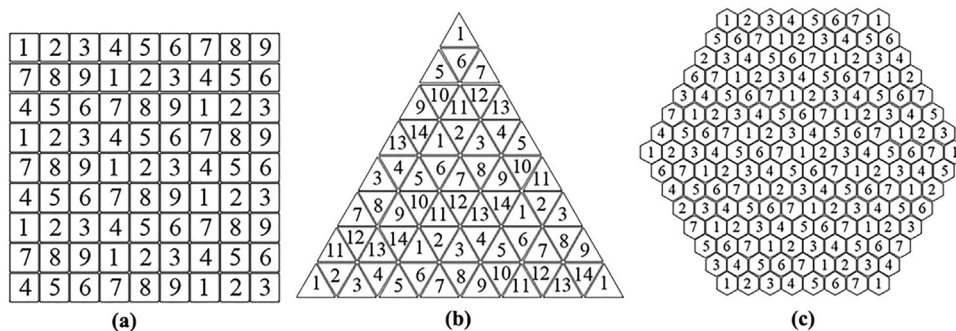


Figure 10. According to the adjacent vertices of each electrode with its neighbor, we can observe that in the case of a square geometry 9 are needed, 14 in the case of a triangle geometry, and 7 for the hexagon geometry. Reproduced under the terms of the CC-BY license.^[69] Copyright 2020, the Authors. Published by AIP Publishing.

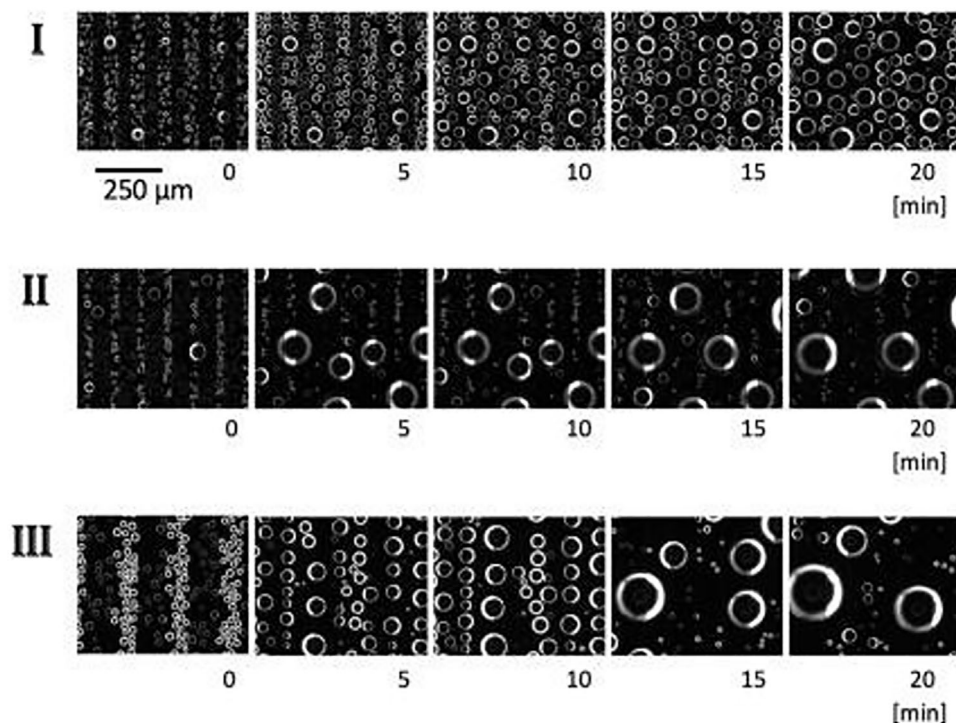


Figure 11. Photograph of droplet growth and coalescence on the device surface. Reproduced with permission.^[59] Copyright 2020, AIP Publishing.

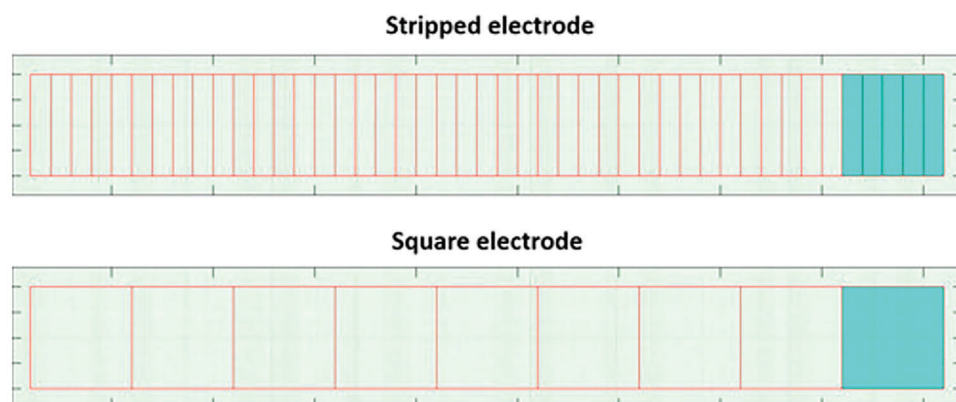


Figure 12. Differences design between stripped electrode and square electrode shapes. Reproduced with permission.^[12] Copyright 2020, AIP Publishing.

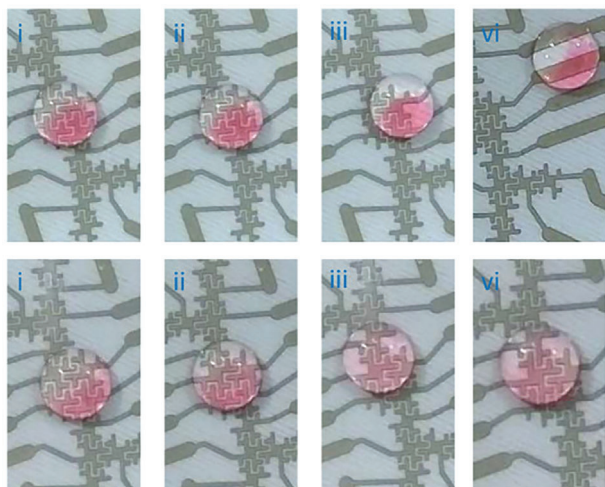


Figure 13. Images taken at times 1.5, 3.5, 5.5, and 25 s respectively showing the homogenization process of the two volumes. Reproduced with permission.^[72] Copyright 2021, Elsevier.

More complex electrode geometries not only move, split or recombine the samples. There are electrodes designs capable to achieve droplet mixing. For instance, Chen et al. in 2021 designed an EWOD device with fylfot crosslike flake electrodes (**Figure 13**) to mix two samples.^[72] The device was able to mix two liquids efficiently by oscillating the droplet as it moved across the electrodes.

As it has been mentioned, the geometry of the electrodes has a major impact on the velocity, directionality, and manipulation of droplet volumes (droplet fusion and fission). However, there are other important features to take into consideration. The method used to create the electrode formation must be appropriate to the material used and the substrate used. A smaller electrode spacing increases the efficiency of the electrostatic forces of the device (Equation (11)). This fact implies that the techniques for electrode deposition, the materials used and the substrate on which the electrodes are defined are of great importance. For example, in inkjet printing on substrates such as paper or synthetic polymers, where materials exhibit capillarity and therefore, a huge dispersion component, can difficult the achievement of small gaps without electrode-to-electrode contact. In addition, the use of conductive inks involves curing at quite high temperatures. The ink must meet two conditions: 1) its rheological characteristics must be compatible with the substrate to obtain accurate patterns and 2) the substrate must withstand the curing temperature of the ink.

4.3. Dielectric Layer

The existence of the dielectric layer between the electrodes and the conductive liquid produces the capacitor effect. This generates an electrostatic potential difference distributed around them when the system is charged. The dielectric layer is critical in the optimal operation of the EWOD device.^[73]

Dielectrics with high dielectric constant such as silicon dioxide (SiO_2) (dielectric constant 3.7),^[74] aluminum oxide (Al_2O_3)

(dielectric constant 9.34),^[75] and tantalum pentoxide (Ta_2O_5) (dielectric constant 71.62) have been used.^[76]

Khan et al. designed an EWOD device with SiO_2 as the dielectric layer.^[74] Two deposition methods, electron beam and sputtering, were evaluated in the study. The thicknesses achieved were 400 nm in both methods, with 120 V driving voltage. According to their results, the sputtering creates a dielectric layer more resistant to electrical breakdown because it has fewer surface irregularities. A device with a more break-resistant dielectric layer allows for a wider range of CA change.

Ribet et al. achieved a 10 nm thick aluminum oxide dielectric layer by plasma-enhanced chemical vapor deposition.^[75] The device presented a very low driving voltage (18–20 V) due to the reduced dielectric thickness and the high dielectric constant of aluminum oxide. Chen et al.^[76] took advantage of the high dielectric constant of Ta_2O_5 to achieve by anodization a 165 nm thick layer. This device works with a voltage of 25 V, being able to decrease the CA from 115° to 92° . High dielectric constant materials enable the deposition of reduced thickness when building the dielectric layer. However, complex manufacturing technologies are required, making it difficult to scale beyond the laboratory. For this reason, current studies are focusing on new manufacturing methods. In 2020, Yi et al. used a 10 μm stretched Parafilm layer but with a 140 V DC minimum driving voltage.^[77] However, the most used manufacturing method to deposit dielectric layers is spin coating, since it allows a wide variety of materials to be deposited. **Table 1** compares recent works that uses spin coating to create the dielectric layer.

SU-8 and polydimethylsiloxane (PDMS) are the two common materials deposited using this method, since both share a reasonable dielectric constant (3 for SU8 and 2.3 for PDMS) and are well known in conventional microfluidics manufacturing processes. Ciou et al. designed a device which required between 140 and 180 V driving voltage due to the use of 1.8 μm thick SU8 dielectric layer manufactured by spin coating.^[85] Basu et al. used a 15 μm thick graphene oxide-PDMS composite as dielectric layer^[67] and characterized higher values of the dielectric constant, higher breakdown electric field, and lower actuation voltages than a single PDMS dielectric layer. Although these materials can be applied by spin coating and are biocompatible, they are not biodegradable.

Zhang et al. used a combination of cellulose triacetate (CTA) and poly(lactic-co-glycolic acid) (PLGA) at 7% and 2% respectively and achieved a 2 μm dielectric layer by spin coating at 5000 rpm for 5 min.^[89] This CTA/PLGA combination doubles SU-8 or PDMS dielectric constant 6 F m^{-1} and the driving voltage of the device was reduced to 60 V.

The researchers have also focused on novel materials with higher dielectric constants. For instance, Narasimhan et al. incorporated an ionic gel, with 12 F m^{-1} as dielectric material in their EWOD device.^[21] The thicknesses studied ranged from 18 to 5 μm and the driving voltage 70 V.

Even though, spin coating is a technique that provides more flexibility in terms of materials and less requirements in terms of setup, the minimum achievable thickness is around 1 μm . Therefore, thicker layers cause a lower capacitance in spin-coated dielectric layer devices, resulting in less efficient devices.^[92] Authors have tested alternatives to decrease the thickness, Clement

Table 1. Different spin coated dielectric layers.

Material	Dielectric constant	Thickness	Voltage	Author and ref.
SU-8	3	4 μm	0–350 V DC	Ciou et al. ^[78]
SU-8	3	15 μm	0–100 V DC	Wang et al. ^[79]
Si ₃ N ₄	7.2	35 μm	70 V DC	Torabina et al. ^[80]
AZ 1500 photoresist	4.03	5 μm	14,8 V DC	Li et al. ^[81]
SU-8	3	500 nm	220 V AC	Chao et al. ^[82]
Cyanoethyl pullulan	18	6 μm	100 V DC	Yu et al. ^[83]
PDMS	2.35	2 μm	160–360 V DC	Bansal et al. ^[84]
PDMS	2.35	500 nm	275 V DC	Jain et al. ^[56]
Ion gel	12	N/A	0–80 V DC	Narasimhan et al. ^[21]
SU-8	3	4 μm	0–350 V DC	Ciou et al. ^[85]
SU-8	3	15 μm	0–100 V DC	Wang et al. ^[86]
PDMS	2.35	8 μm	0–250 V DC	Li et al. ^[87]
SU-8	3	10 μm	200 V AC	Nahar et al. ^[17]
Cellulose triacetate/PLGA	6	1.8 μm	110 V DC	Kojima et al. ^[82]
PDMS	2.35	N/A	1500–5000 V DC	Chen et al. ^[88]
Cellulose triacetate/PLGA	3	6 μm	40–100 V DC	Zhand et al. ^[89]
Ion gel	3	5 μm	150 V AC	Clement et al. ^[53]
SU-8	3.8	2 μm	130 V AC	Yi et al. ^[77]
SU-8	3	2.5 μm	0–100 V DC	Chae et al. ^[73]
SU-8	3	2 μm	10–100 V DC	Chen et al. ^[76]
SU-8	3	N/A	100 V DC	Huang et al. ^[90]
HN-008N	3	500 nm	175 V DC	Yang et al. ^[91]
PDMS + graphene oxide	3.2	15 μm	100 V DC	Basu et al. ^[66]

et al. used the same ionic gel and reduced the thickness of the dielectric layer to 500 nm using dip-coating techniques.^[92]

Recently, new material deposition technologies have appeared such as ink-jet printing. Jet printing could form thin layers of dielectric materials that improve the capacitance of the devices and provide more material flexibility. For instance, nowadays SU-8 can be ink jet printed. This may facilitate the fabrication of the devices by printing the electrodes and the dielectric layer with the same technology.^[93]

High voltage devices are the main bottleneck for the commercialization of EWOD technology.^[73] This is mainly because the high-voltage power supply can be heavy, which limits its use as a portable device, the main requirement of point-of-care devices. The capacitance is key to lower this voltage. A higher capacitance allows the achievement of the same CA reduction with less voltage (Equation (7)) and consequently lower probability of dielectric breakdown. In order to obtain high capacitances, materials with high dielectric constant and/or low layer thicknesses are used (Equation (8)). However, in the choice of material, the first criterion is the deposition method available. Generally, complex methods (that involve the use of a cleanroom) allow the deposition of nanometer layers with materials with higher dielectric constants. In this way, there is a need to explore new materials that can be deposited with more simple methods and that have high dielectric constants. Finally, the stiffness of the dielectric layer must not be forgotten. A device with an elastic substrate designed to adapt to a surface requires a dielectric with the same characteristics. However, the use of these elastic materials will affect the

efficiency of the device due to the appearance of wetting ridges. Instead, it is desirable to use a rigid dielectric material in rigid devices for higher efficiency.

4.4. Hydrophobic Layer

The movement of the droplet on the surface of the device occurs when the imbalance of forces between the contact line on the connected electrode and the contact line on the unconnected electrode exceeds the drag or adhesion forces.^[51] Therefore, an electrical pulse strong enough is needed to overcome these forces and to create the motion of the droplet on the surface. A low surface energy surface decreases the force needed to initiate the droplet movement with a lower voltage.^[22] Therefore, the last layer of an EWOD device uses materials with low surface energy, especially fluorinated materials such as Teflon or Cytop. In addition, this layer must be thin enough, in the order of nanometers to avoid increasing the required voltage to drive the device.^[73]

Chae et al. studied different Cytop and Teflon thicknesses achieved by spin coating. A 3 nm Teflon layer presented a 116° CA and a 7 nm Cytop layer 111° CA. According to the results about the surface wettability, the CA hysteresis, and the EWOD performance, the optimum hydrophobic layer thickness was found to be 12 nm.^[73]

Huang et al. designed a device to manipulate mouse embryos with a Teflon coating.^[90] The thickness of the hydrophobic coating was 20 nm and the device presented a CA of 120°. Wang et al.

designed an EWOD device to handle cell cultures with a Teflon coating.^[16] By spin coating they achieved a 60 nm Teflon layer with a 121.6° CA. At a voltage of 100 V DC, CA reduction up to 60° was observed. Seo et al. designed an EWOD-based liquid lens with 70 nm Cytop layer spin coated.^[94] The initial CA was 110° and the minimum CA was 72°, under 45 V DC. Zhang et al. designed an EWOD device with a CTA/PLGA layer, to which they incorporated carbon tetrafluoride (CF₄) and silicon oil.^[89] The combination of CF₄ and the roughness of the CTA/PLGA surface allows a CA of 160° to be displayed. Without this CF₄ treatment, the initial CA was 60°. The combination of CTA/PLGA provides a roughness that allows CA above 120° to be observed.

Even though Fluorinated materials present remarkable contact angles, it should not be forgotten that these materials are not safe for the environment, since they are active contributors to the global warming. There is a need to explore alternative materials that are ecologically sustainable. Jain et al. designed an EWOD device with a hybrid dielectric-hydrophobic PDMS coating.^[47] By spin coating, a 15 μm PDMS layer from 160 to 360 V driving voltages were used in their study. These high voltages are due to the high layer thicknesses. If smaller thicknesses were used, the drive voltages could be greatly reduced.

Another way to increase the contact angle is by modifying the surface roughness.^[95] Yasmeen et al. designed an EWOD device by mixing paraffin or PDMS with granular materials.^[96] These granular materials, such as sugar or albumin, create roughness that increases the contact angle due to the Cassie-Baxter effect, and drops with a CA of 160° can be observed. Kim et al. designed a conventional EWOD device with 85 nm diameter Teflon-coated ZnO nanorods to study their CA change.^[97] The combination of roughness due to the ZnO nanorods and the Teflon coating allows observing an initial CA of 138°. Wang et al. used an EWOD device with a rough surface to study the variations of the contact angle, the travel distance achieved and the sliding direction of a droplet.^[98] It was shown that surface roughness can increase the CA of a droplet, but there may be differences in the CA of left and right. Also, in its displacement on a nonhomogeneous surface, there may be irregularities on the surface that can increase the adhesion forces. However, on a surface with ridges whose roughness exceeds the values indicated by Ra (arithmetic average of the absolute values of the profile height deviations from the mean line), the sliding direction of the droplet can be controlled and the sliding distance can be increased.

Different characteristics of hydrophobic and hydrophilic materials on the surface of the devices can be examined in order to achieve lower driving voltages or increased velocities. Sun et al. designed an EWOD device with periodic hydrophilic semicircular regions of microscopic size on a hydrophobic background that they called anisotropic ratchet carriers (ARCs).^[99] These ARCs had Cytop as the hydrophobic part and SiN₂ as the hydrophilic part (Figure 14). The droplet was moved over this surface at 13 mm s⁻¹ with only two electrodes, using an AC at 50 Hz.

Mogi et al. designed a coplanar EWOD device with dimpled structures.^[63] These dimpled structures allow a better definition of the droplet direction, avoiding spontaneous out-of-control movements (Figure 15).

However, roughness may not be useful in coplanar EWOD devices since it can increase the force required for the droplet

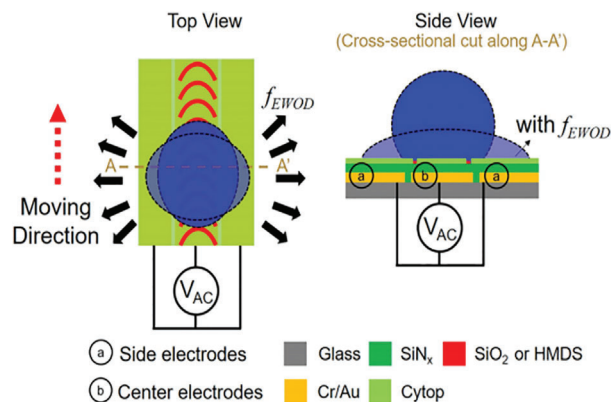


Figure 14. Top and cross-sectional view of the EWOD device with rackets made of SiO₂ and Cy-top. Reproduced with permission.^[99] Copyright 2020, AIP Publishing.

motion. An example of this is found in the work of Shirinkami et al.^[100]

In their design, they measured the height between the electrode and the substrate after the incorporation of the hydrophobic Cytop layer. The measured height of this layer was 85 nm, which is an obstacle in the droplet motion and increases the adhesion and the drag force. With a chemical-mechanical polishing step, they were able to smooth the surface and then increase the speed up to 100% in 3.5 μL samples.

The hydrophobic layer is the component that provides the highest possible initial CA in the device. This can be achieved by two actions: either increasing the surface roughness or using highly hydrophobic materials on the surface. Micro- and nanoscale surface roughness can increase the CA, but has other drawbacks such as increased friction forces (Equation (13)) and irregularities between the CAs observed at the ends of a static droplet.

However, it is possible to design patterns on the surface (such as channels or rackets) that can facilitate directional movement. This enhances the hydrostatic force component (Equation (12)). Generally, the materials that exhibit high hydrophobicity have a high environmental impact. It is worth mentioning here that these devices may be designed for point-of-care use. This implies single-use devices. The use of materials with high environmental impact would be recommended in such devices. There is a need to explore materials with high hydrophobicity and no environmental drawbacks.

In addition, most authors do not consider the hydrophobic coating effects on the capacitance of their devices, even if it is a small effect. This effect should not be neglected when exploring new materials.

5. EWOD Devices Applications

EWOD devices have seen an exponential increase in their use and their commercialization since 2000.^[101] Conventional EWOD devices have their market in the use of liquid lenses. Mobile phones are already using this technology in their lenses, as for example the Xiaomi Mi Mix mobile. On the other hand,

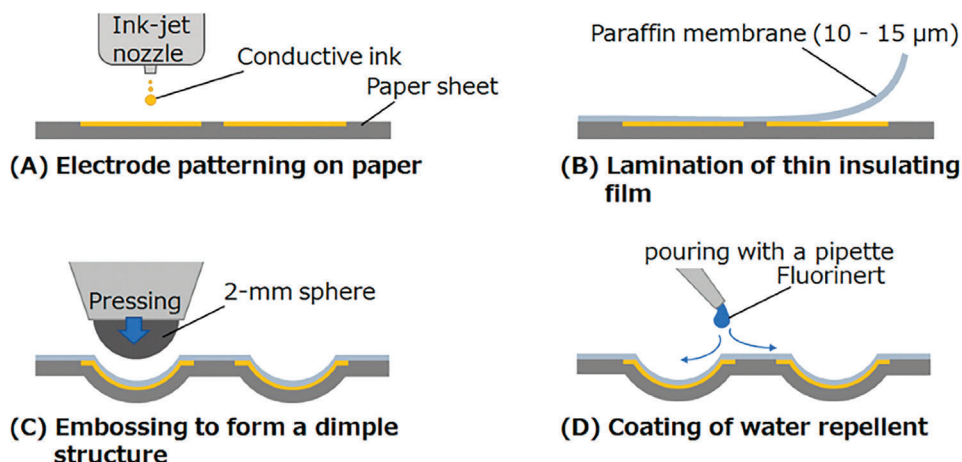


Figure 15. Fabrication process of the EWOD coplanar device with dimpled structures. These structures are formed by pressure on a flexible substrate. Reproduced with permission under the terms of the CC-BY license.^[63] Copyright 2019, the Authors. Published by MDPI.

Digital microfluidics is of great commercial interest in analytical and biomedical devices. For example, Illumina's NeoPrep Library Prep System uses co-planar EWOD-driven digital microfluidics to manipulate biological samples. A side from commercial success, research is continuously working on the development of novel EWOD devices in the following areas:

5.1. Lens Applications

Manipulating the CA of a droplet by EWOD affects the value of the reflection of light passing through the liquid. This fact allows a tunable focal shift across different electric potentials,^[5] avoiding the use of complicated mechanisms to precisely manipulate solid lenses.^[102] Furthermore, liquid lenses have the advantage of being flexible. Li et al. presented an EWOD device that doubles as a microlens but was also flexible.^[102] This device was compatible with curved surfaces without adding distortion to the image captured through the lens. The lens allowed to change the focal length from 38 to 29 mm on flat surfaces and from 41 to 31 mm on curved surfaces and could also provide zoom (**Figure 16**).

Kopp et al. designed an EWOD device that can handle two liquids in an oily environment.^[103] **Figure 17** shows the digital change of the zoom lens by the independent modulation of the two drops within an oily environment.

When dealing with optical lenses, optical aberrations are defects that appear in the images captured. The most common problem is chromatic aberration. Song et al.^[104] partially eliminated these chromatic aberrations creating a triple liquid lens EWOD with a larger numerical aperture (**Figure 18**).

Even though, there are other devices that add the zoom capability to the focusing capability without adding more lenses. Park et al. designed an EWOD device with the ability to focus and zoom using a single liquid lens.^[105] **Figure 19** shows the two completely different mechanisms that the device presents. First, the conventional EWOD device modulates the curvature of its surface to adapt the focus. Second, the liquid chamber mechanism is capable of incorporating or capturing liquid from the lens, increasing or decreasing the thickness of the liquid lens.

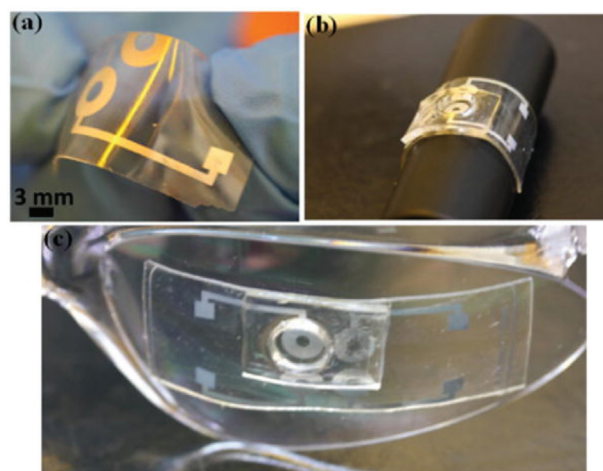


Figure 16. Flexible liquid slow device presented by Li et al. a) The PDMS substrate allows it to be folded without difficulty. b) Adaptation of the device to a curved surface. c) Adaptation of the device on a spectacle lens. Reproduced with permission under the terms of the CC-BY license.^[102] Copyright 2014, the Authors. Published by MDPI.

Liquid lenses are presented as an innovation in the field of optics. It allows to have the same characteristics as conventional solid lenses while eliminating the mechanical parts that are susceptible to failures. But, they have the disadvantage of being dependent on an electrical source.

5.2. Analytical Applications

Digital microfluidics has the ability to precisely manipulate and move small, discrete volumes of fluids. Therefore, EWOD is one of the most promising methods to miniaturize analytical tools. In the use of EWOD as digital microfluidics, we can differentiate several purposes:^[106] cell cultures manipulation,^[107] chemical reactions,^[80] sample preparation,^[108] chemical analysis,^[109] and biological analysis.^[110]

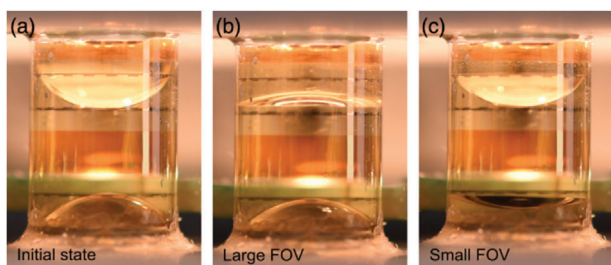


Figure 17. EWOD-based optical device with two liquid lenses in an oily environment. Reproduced with permission under the terms of the CC-BY license.^[103] Copyright 2017, the Authors. Published by Optica Publishing Group.

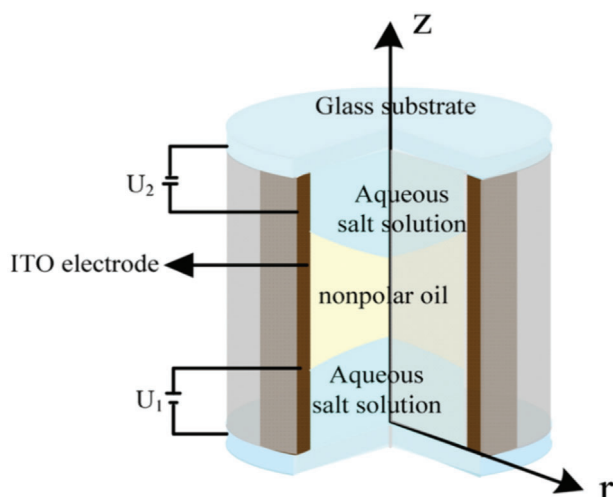


Figure 18. Schematic of the triple liquid device of Song et al. Reproduced under the terms of the CC-BY license.^[104] Copyright 2020, the Authors. Published by Springer Nature.

5.3. Cell Cultures Manipulation

One of the main problems when working with cell cultures is the maintenance of a sterile environment. When handling culture media, sterile materials should always be used to avoid contamination. The use of digital microfluidics allows the use of a single sterile platform for sample handling without the need for additional instruments. Li designed an EWOD-based microfluidic device for the mouse embryo manipulation.^[107] They manipulated two-cell mouse embryos up to a blastocyst. The embryo culture is a more complex protocol than the conventional cell culture and therefore requires special care in the materials chosen for device fabrication.

Another work related to the mouse embryos, Alias et al. extracted cell-free DNA from a mouse embryo culture.^[111] This method achieves an extraction yield of 23%, compared to 14% achieved for the conventional method. The use of a digital microfluidic device provides the ability to handle small volumes with almost no dead-end fluid losses, such as it might occur with the use of micropipettes due to capillary forces or conventional microfluidics. Lee et al. designed an EWOD-based digital microfluidic device that simultaneously detects two growth factors in embryo cultures with human culture medium.^[112] The analy-

sis of these growth factors in these cultures faces two challenges: the requirement of a dose on the order of a few microliters and the low concentration of these growth factors. Traditional methods, such as enzyme-linked immunosorbent assay (ELISA), require larger quantities. The use of digital microfluidics allows the use of a microliter volume and the combination with antibodies without sample loss.

5.4. Chemical Reactions

Some samples undergoing analysis contain potentially hazardous substances. Lee et al. designed a digital microfluidic device based on EWOD coupled to mass spectrometry (MS) and gas chromatography-mass spectrometry. The objective was the analysis of highly toxic substances used in chemical warfare.^[113] This device allows samples to be handled, prepared, and transported to analysis and waste areas without human exposure to the highly toxic substances.

Wang et al. designed a device for handling radioisotope substances. This device reduces the amount of radiation shielding for technicians and reduces handling times for analyses such as positron emission tomography, where short-lived radioisotopes are needed.^[114]

5.5. Biological Analysis

In biological or medical analysis, the EWOD device offers the capability to handle very small samples. This avoids contamination of samples and increases the safety of the technicians in charge of handling them. The recent Coronavirus disease 2019 (COVID19) pandemic has raised the focus of clinical personnel safety. Health care workers and scientists have had to work on the COVID19 study with a shortage of personal protective equipment. Jain et al. designed an EWOD platform that allows the COVID19 sample to be fused with the analysis reagent to transport the resulting solution to the analysis site.^[115] Handling COVID19 samples with EWOD safeguards the safety of scientific/healthcare personnel and avoids contamination of other samples (Figure 20).

In a similar manner, Petralia et al. designed an EWOD-based microfluidic device to add the necessary reagents to perform real-time polymerase chain reaction (RT-PCR) in 96-well sample cartridges.^[116] This microfluidic system allows RT-PCR analysis on many simultaneous samples automatically. In addition, it avoids crosscontamination or technician errors. Another approach was presented by Rui et al. to perform PCR using the droplet itself as a biological reactor.^[110] The use of droplets as bioreactors allows the use of PCR with minimal DNA concentration, one strand per droplet, with only the site of interest being amplified using specific primers. Once the sequence of interest is amplified, it can be easily detected by fluorescence.

Wheeler et al. designed a parallel-plate device for sample preparation and analysis by matrix-assisted laser desorption/ionization mass spectrometry.^[117] The use of the EWOD parallel plate allowed the handling of very small volumes, the mixing with other indicators, and the sample transport. The use of digital microfluidics avoids loss of sample volume. Min et al. presented a single-plate EWOD device for ion analysis.^[118] In the fabrication

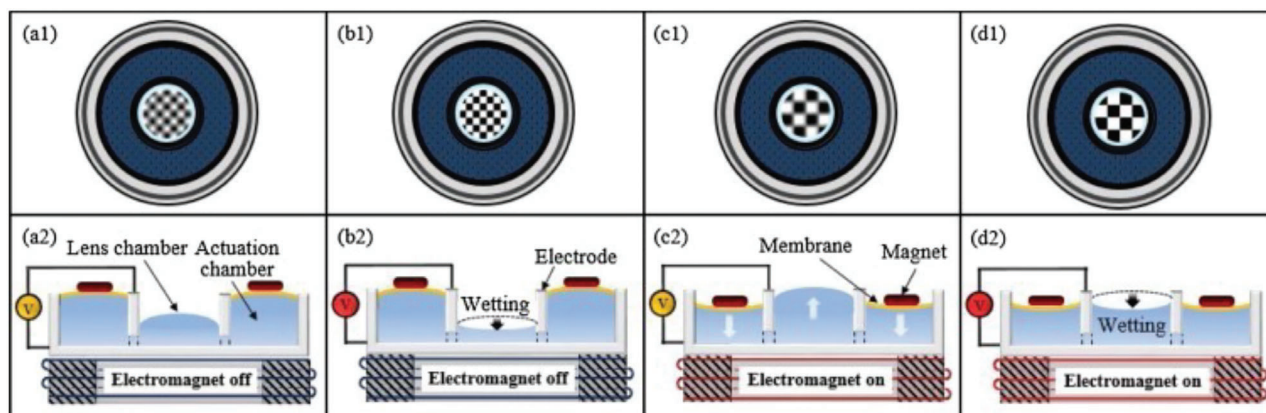


Figure 19. Schematic diagram of the functioning of the liquid lens presented by Park. Reproduced with permission.^[105] Copyright 2018, Elsevier.

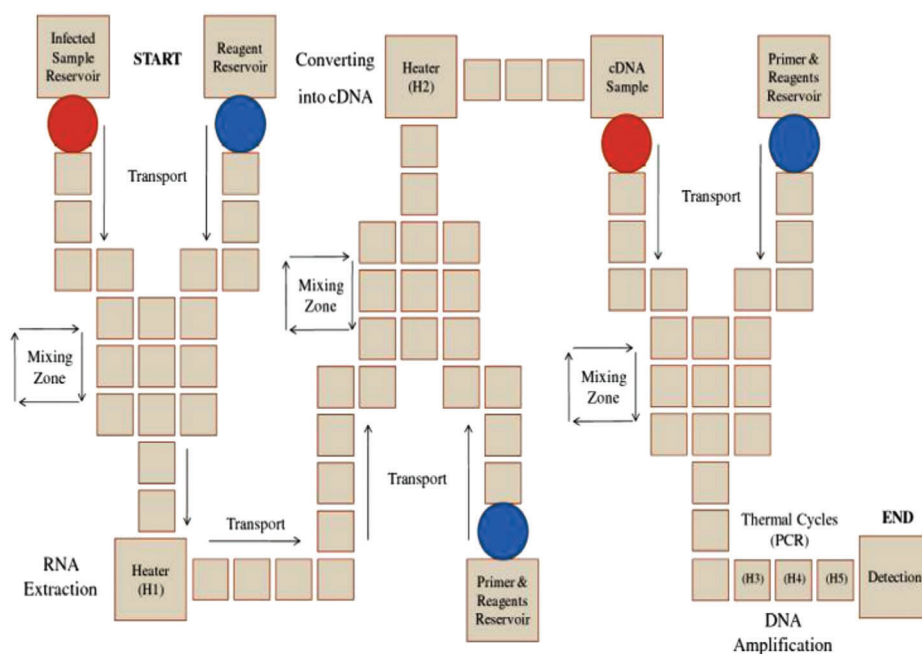


Figure 20. Digital microfluidic device to perform each step of a PCR without the need for manual sample handling. Reproduced under the terms of the CC-BY license.^[115] Copyright 2020, the Authors. Published by Springer Nature.

of the device, ion-selective electrode sensors were capable of performing selective detection of ions along with other interfering ions.

Digital microfluidics can also be used for immobilization of particles on the device surface in order to functionalize it. Malic et al. demonstrate a digital microfluidic device for simultaneous immobilization of different DNA probes on the surface with the aim of creating dynamically configurable surface plasma resonance biochips.^[119] This technique demonstrates the ability to regulate probe density and orientation.

5.6. Other EWOD Applications

The ability to move discrete fluids as a droplet can present wide variety of uses. One of the most studied case is the cooling of

surfaces by droplets of coolants on demand.^[120–123] Ahmad et al. designed a method for cooling hot spots in electronic devices.^[78] Current electronic devices are capable of performing a wide variety of specific functions, resulting in nonuniform surface temperature. To specifically cool certain hot spots, an EWOD device moves coolant droplets to specific areas to cool these areas. The use of refrigerants on demand can make refrigeration systems more efficient with lower consumption.

Capturing moisture from a surface is another potential application of the EWOD devices. Yan et al. presents an EWOD device that has the ability to capture ambient moisture through the nucleation of droplets that occur on a surface due to condensation.^[124] The water capture capacity increases by 138.96%, 171.87%, and 220.43% with the use of 20, 40, and 60 V voltages, respectively. This application can also be used to create self-cleaning surfaces.

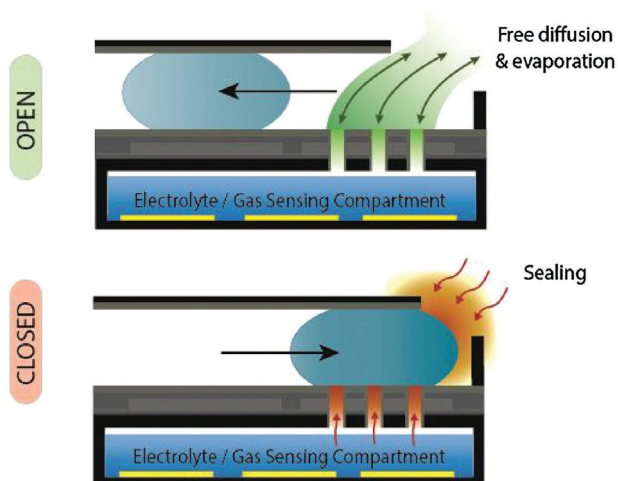


Figure 21. Working principle of the EWOD device as a gas valve presented by Ribet et al. Reproduced with permission.^[75] Copyright 2020, Elsevier.

Manipulation of a droplet also allows its use as a gas valve. The movement of a droplet can open or close a gas inlet opening. Ribet et al. designed an EWOD device that is used to prevent evaporation of electrolytes used in electrochemical gas sensors.^[75] The EWOD device has the ability to move droplets toward the electrolyte inlets, blocking diffusion when necessary. This prevents evaporation of the electrolyte when it is not needed. **Figure 21** shows that system can extend the life of this type of sensor, since there is no possibility of refilling and recalibration.

6. Conclusions

The EWOD effect describes the change in the contact angle between a solid and an ionic liquid due to a potential difference applied between them. This phenomenon allows the creation of different devices for multiple applications. Although there are already some commercial products that make use of this EWOD effect, this review article has revealed certain shortcomings or disadvantages in the devices created on this basis. The main limitations are the need to use high voltages for operation and, the use of harmful environmental impact materials in their manufacturing. The material used in the individual layers of the EWOD device depends mainly on the function of the layer itself in the device and the application of the device. The substrate layer may require transparency and flexibility to adapt to nonflat structures, which precludes the use of common materials such as PCB and glass. In this case, there has been a need to find cheap, biocompatible and biodegradable materials that meet these requirements. The conductive layer has the widest range of possible materials. It has been found that there are a multitude of methods for manufacturing this layer and that the efficiency of the device depends mainly on the geometry and the distance between electrodes, rather than on the material from which it is made. In this case, the novelty would be to design efficient geometries using the least amount of material to minimize costs in this layer. With regard to the dielectric layer, it is clear that the material used must have a high dielectric constant in order to create the thinnest possible layer so that the device can work with lower voltage without

losing efficiency. In this sense, it has been observed that the materials that meet these requirements require manufacturing methods that limit the scalability of the production of the devices on an industrial level. A simple method such as spin coating would enable the manufacturing this type of devices without the need for complex installations, which would facilitate its implementation in places with scarce resources. But the material to be used with this method is yet to be discovered and initial attempts are being done in more biocompatible and ecofriendly materials. Regarding to the hydrophobic layer, materials are sought for providing the lowest surface energy. In the literature, novel strategies use the creation of surfaces with nanoroughness to avoid harmful materials, but although they increase the contact angle, they difficult the droplet to motion. Currently, the main problem related to this layer is still the type of materials used, which are usually fluorocarbons, whose harmful environmental impact is well known.

Therefore, although devices based on the EWOD effect have great potential, the research now focuses on developing manufacturing processes that comply with the concepts of eco-design and bioeconomy and achieve the accuracy required.

7. Experimental Section

In this review the current trends were focused in the use of novel materials, especially those that are environmental friendly and new manufacturing techniques that have recently appeared and are more sustainable.

A methodical search was carried out in the SCOPUS and Google Scholar databases, using the keywords “electrowetting-on-dielectric,” “EWOD,” “digital microfluidics.” The criteria for inclusion of papers in the review are: 1) studies published not earlier than 2017, 2) their novelty in the use of a material in one of its layers or novel manufacturing processes more sustainable, and 3) it is a clear example of how to use a material in a certain way to meet the needs of EWOD devices.

Acknowledgements

The authors would like to acknowledge funding by Spain’s Ministry of Science and Innovation and Spain’s State Research Agency: PID2020-114070RB-I00 (CELLECOPROD).

Conflict of Interest

The authors declare no conflict of interest.

Keywords

digital microfluidics, electrowetting-on-dielectrics, EWOD, liquid lenses

Received: March 17, 2022
Revised: September 2, 2022
Published online:

- [1] G. Lippmann, *Ann. Chim. Phys* **1875**, 5, 494.
- [2] A. Frumkin, *J. Colloid Sci.* **1946**, 1, 277.
- [3] G. Beni, S. Hackwood, *Appl. Phys. Lett.* **1981**, 38, 207.
- [4] M. Vallet, B. Berge, L. Vovelle, *Polymer (Guildford, Engl.)* **1996**, 37, 12.

- [5] M. Kang, R. Yue, *J. Adhes. Sci. Technol.* **2012**, 26, 1941.
- [6] J. Zeng, T. Korsmeyer, *Lab Chip* **2004**, 4, 265.
- [7] U. C. Yi, C. J. Kim, *J. Micromech. Microeng.* **2006**, 16, 2053.
- [8] J. Heikenfeld, M. Dhindsa, *J. Adhes. Sci. Technol.* **2008**, 22, 319.
- [9] N. Verplanck, Y. Coffinier, V. Thomy, R. Boukherroub, *Nanoscale Res. Lett.* **2007**, 2, 577.
- [10] J. Theisen, L. Davoust, *Microfluid. Nanofluid.* **2015**, 18, 1373.
- [11] H. Feng, Z. Yi, R. Yang, X. Qin, S. Shen, W. Zeng, L. Shui, G. Zhou, C. Zhang, *Micromachines* **2020**, 11, 1067.
- [12] Y. Guan, M. Zhu, B. Li, J. Tu, L. Xing, X. Chen, *Phys. Fluids* **2020**, 32, 012010.
- [13] J.-T. Cheng, C.-L. Chen, **2010**, 14, 63.
- [14] K. N. Nampoothiri, M. S. Seshasayee, V. Srinivasan, M. S. Bobji, P. Sen, *Sens. Actuators, B* **2018**, 273, 862.
- [15] L.-S. Jang, C.-Y. Hsu, C.-H. Chen, *Biomed. Microdevices* **2009**, 11, 1029.
- [16] W. Wang, X. Rui, W. Sheng, Q. Wang, Q. Wang, K. Zhang, A. Riaud, J. Zhou, *Sens. Actuators, B* **2020**, 324, 128763.
- [17] M. M. Nahar, J. B. Nikapitiya, S. M. You, H. Moon, *Micromachines* **2016**, 7, 71.
- [18] Q. Wei, W. Yao, L. e Gu, B. Fan, Y. Gao, L. i Yang, Y. Zhao, C. Che, *Biomicrofluidics* **2021**, 15, 014107.
- [19] J. Lienemann, A. Greiner, J. G. Korvink, *IEEE Trans. Comput. Des. Integr. Circuits Syst.* **2006**, 25, 234.
- [20] H. Moon, S. K. Cho, R. L. Garrell, C. J. Kim, *J. Appl. Phys.* **2002**, 92, 4080.
- [21] V. Narasimhan, S. Y. Park, *Langmuir* **2015**, 31, 8512.
- [22] Q. Ni, D. E. Capecchi, N. B. Crane, *Microfluid. Nanofluid.* **2015**, 19, 181.
- [23] L. Mats, A. Bramwell, J. Dupont, G. Liu, R. Oleschuk, *Microelectron. Eng.* **2015**, 148, 91.
- [24] N. Rajabi, A. Dolatabadi, *Colloids Surfaces A Physicochem. Eng. Asp.* **2010**, 365, 230.
- [25] Q. Vo, T. Tran, *J. Fluid Mech.* **2021**, 925, A19.
- [26] A. Quinn, R. Sedev, J. Ralston, *J. Phys. Chem. B* **2005**, 109, 6268.
- [27] D. Sun, K. Böhringer, *Micromachines* **2019**, 10, 101.
- [28] J. F. Oliver, C. Huh, S. G. Mason, *J. Adhes.* **1976**, 8, 223.
- [29] G. Wolansky, A. Marmur, *Colloids Surf., A* **1999**, 156, 381.
- [30] K. Lamnawar, M. Bousmina, A. Maazouz, *Macromolecules* **2012**, 45, 441.
- [31] B. He, N. A. Patankar, J. Lee, *Langmuir* **2003**, 12, 4999.
- [32] A. C. Miller, J. C. Berg, *Adhes. Sci. Eng.* **2012**, 16, 5.
- [33] R. N. Wenzel, *Ind. Eng. Chem.* **1936**, 28, 988.
- [34] D. M. Spori, T. Drobek, S. Zürcher, M. Ochsner, C. Sprecher, A. Mühlebach, N. D. Spencer, *Langmuir* **2008**, 24, 5411.
- [35] D. Kim, N. M. Pugno, S. Ryu, *Sci. Rep.* **2016**, 6, 37813.
- [36] Q. Zheng, C. Lü, *Procedia IUTAM* **2014**, 10, 462.
- [37] A. B. D. Cassie, S. Baxter, *Trans. Faraday Soc.* **1944**, 40, 546.
- [38] S. Popinet, *Annu. Rev. Fluid Mech.* **2018**, 50, 49.
- [39] E. Bormashenko, V. Starov, *Colloid Polym. Sci.* **2013**, 291, 343.
- [40] N. A. Patankar, *Langmuir* **2004**, 20, 8209.
- [41] F. Mugele, J.-C. Baret, *J. Phys.: Condens. Matter* **2005**, 17, R705.
- [42] P.-G. de Gennes, F. Brochard-Wyart, D. Quéré, *Capillarity Wetting Phenom.* **2004**, 315, 139.
- [43] M. G. Pollack, R. B. Fair, A. D. Shenderov, *Appl. Phys. Lett.* **2000**, 77, 1725.
- [44] M. A. Islam, A. Y. Tong, *Numer. Heat Transfer, Part A* **2017**, 71, 805.
- [45] J.-T. Cheng, C.-L. Chen, *Exp. Fluids* **2010**, 49, 1349.
- [46] J. Berthier, P. Dubois, P. Clementz, P. Claustrate, C. Peponnet, Y. Fouillet, *Sens. Actuators, A* **2007**, 134, 471.
- [47] V. Jain, A. Hole, R. Deshmukh, R. Patrikar, *Sens. Actuators, A* **2017**, 263, 224.
- [48] F. Mugele, *Soft Matter* **2009**, 5, 13377.
- [49] S. R. Barman, S. R. Klan, S. Chatterjee, S. Saha, D. Choi, S. Lee, Z. H. Lin, *J. Food Drug Anal.* **2020**, 28, 595.
- [50] W. C. Nelson, P. Sen, C. J. C. J. Kim, *Langmuir* **2011**, 27, 10319.
- [51] T. Roques-Carmes, R. A. Hayes, B. J. Feenstra, L. J. M. Schlangen, *J. Appl. Phys.* **2004**, 95, 4389.
- [52] G. Mchale, N. Gao, G. G. Wells, H. Barrio-Zhang, R. Ledesma-Aguilar, *Langmuir* **2022**, 38, 4425.
- [53] C. E. Clement, S. K. Thio, S.-Y. Park, *Sens. Actuators, B* **2017**, 240, 909.
- [54] Y. Guan, A. Y. Tong, *J. Heat Transfer* **2015**, 137, 9.
- [55] V. Jain, V. Devarasetty, R. Patrikar, *J. Electrostat.* **2017**, 87, 11.
- [56] V. Jain, T. P. Raj, R. Deshmukh, R. Patrikar, *Microsyst. Technol.* **2017**, 23, 389.
- [57] A. N. Banerjee, S. Qian, S. W. Joo, *J. Colloid Interface Sci.* **2011**, 362, 567.
- [58] J. Li, K. Chang-Jin, *Proc. IEEE Int. Conf. Micro Electro Mech. Syst., IEEE, Seoul, Korea* **2019**, p. 180.
- [59] S. Högnadóttir, K. Kristinsson, H. G. Thormar, K. Leosson, *Appl. Phys. Lett.* **2020**, 116, 073702.
- [60] J. Cao, Q. i An, Z. Liu, M. Jin, Z. Yan, W. Lin, L. Chen, P. Li, X. Wang, G. Zhou, L. Shui, *Sens. Actuators, B* **2019**, 291, 470.
- [61] D. Sun, G. Gomez, K. F. Böhringer, *2019 Solid-State Sensors, Actuators Microsystems Eurosensors XXXIII (TRANSDUCERS EUROSENSORS XXXIII)*, IEEE, Berlin, Germany **2019**, p. 2270.
- [62] K. L. Van Grinsven, A. Ousati Ashtiani, H. Jiang, *Micromachines* **2019**, 10, 464.
- [63] K. Mogi, S. Adachi, N. Takada, T. Inoue, T. Natsume, *Appl. Sci.* **2019**, 9, 2406.
- [64] S. J. Park, B. M. Weon, J. S. Lee, J. Kim, J. H. Je, *Nat. Commun.* **2014**, 5, 1.
- [65] B. Andreotti, J. H. Snoeijer, **2020**, 52, 285.
- [66] M. Basu, V. P. Joshi, S. Das, S. Dasgupta, *J. Electrostat.* **2021**, 109, 103541.
- [67] C. Palma, R. D. Deegan, *Langmuir* **2018**, 34, 3177.
- [68] V. Jain, A. Hole, R. Deshmukh, R. Patrikar, *Sens. Actuators, A* **2017**, 263, 224.
- [69] K. Zhang, W. Wang, C. Li, A. Riaud, J. Zhou, *AIP Adv.* **2020**, 10, 055227.
- [70] Y.-B. Wang, J.-H. Huang, M.-S. Lee, C.-Y. Huang, C.-S. Huang, I. Yamashita, Y.-Y. Tu, W. Hsu, *Microsyst. Technol.* **2017**, 23, 3645.
- [71] R. Lejard-Malki, J. R. M. Follet, A. Vlandas, V. Senez, *Lab Chip* **2018**, 18, 3310.
- [72] Y.-Y. Chen, I.-J. Ting, S.-C. Wang, *J. Taiwan Inst. Chem. Eng.* **2021**, 126, 23.
- [73] J. B. Chae, J. O. Kwon, J. S. Yang, D. Kim, K. Rhee, S. K. Chung, *Sens. Actuators, A* **2014**, 215, 8.
- [74] I. Khan, S. Castelletto, G. Rosengarten, *Mater. Res. Express* **2018**, 5, 076304.
- [75] F. Ribet, L. De Pietro, N. Roxhed, G. R. Stemme, *Sens. Actuators, B* **2018**, 267, 647.
- [76] S. Chen, C.-J. Ī. G. H. Kim, *Sens. Mater.* **2019**, 31, 2861.
- [77] Z. Yi, H. Feng, X. Zhou, L. Shui, *Front. Phys.* **2020**, 8, 193.
- [78] I. Ahmad, M. Pathak, M. K. Khan, *Exp. Therm. Fluid Sci.* **2021**, 125, 110372.
- [79] A. Tröls, S. Clara, B. Jakoby, *Sens. Actuators, A* **2016**, 244, 261.
- [80] M. Torabinia, U. S. Dakarapu, P. Asgari, J. Jeon, H. Moon, *Sens. Actuators, B* **2021**, 330, 129252.
- [81] C. Li, W. Wang, L. Chao, X. Ji, J. Zhou, *J. Microelectromech. Syst.* **2017**, 26, 1449.
- [82] L. Chao, Z. Zeng, K. Zhang, J. Zhou, *IEEE Trans. Dielectr. Electr. Insul.* **2017**, 24, 3132.
- [83] J. Yu, X. Wei, Y. Guo, Z. Zhang, P. Rui, Y. Zhao, W. Zhang, S. Shi, P. Wang, *Lab Chip* **2021**, 21, 284.
- [84] S. Bansal, P. Sen, *J. Colloid Interface Sci.* **2020**, 568, 8.
- [85] Y.-J. Ciou, H.-T. Lee, Y.-W. Lin, D.-J. Yao, *AIP Adv.* **2020**, 10, 125115.
- [86] W. Wang, Q. Wang, K. Zhang, X. Wang, A. Riaud, J. Zhou, *Sens. Actuators, B* **2020**, 312, 127983.

- [87] J. Li, C. Kim, *2019 IEEE 32nd Int. Conf. Micro Electro Mech. Syst.*, IEEE, Seoul, Korea **2019**, p. 180.
- [88] Y. Chen, S. Wang, *Sensors (Basel)* **2018**, *18*, 3228.
- [89] K. Zhang, L. Chao, J. Zhou, *Materials (Basel)* **2018**, *11*, 1332.
- [90] H. Y. Huang, D. F. T. Chang, P. C. Wu, *PLoS One* **2015**, *10*, e0140419.
- [91] G. Yang, H. Chen, B. Tang, A. Henzen, G. Zhou, *Results Phys.* **2021**, *24*, 104161.
- [92] C. E. Clement, D. Jjiang, S. K. Thio, S.-Y. Park, *Mater. (Basel, Switzerland)* **2017**, *10*, 41.
- [93] W. Cui, M. Zhang, X. Duan, W. Pang, D. Zhang, H. Zhang, *Micromachines* **2015**, *6*, 778.
- [94] S. Seo, S. K. Yoo, J. Kim, D. Moon, *2019 Solid-State Sensors Actuators Microsystems Eurosensors XXXIII, TRANSDUCERS 2019 EUROSENSORS XXXIII*, IEEE, Berlin, Germany **2019**, p. 1592.
- [95] W. Barthlott, C. Neinhuis, *Planta* **1997**, *202*, 1.
- [96] S. Yasmeen, J. Yoon, C. H. Moon, R. Khan, H. Ganji, S. Shin, I. K. Oh, H. B. R. Lee, *Langmuir* **2021**, *37*, 5356.
- [97] J.-H. Kim, J.-H. Lee, A. Mirzaei, H. W. Kim, B. T. Tan, P. Wu, S. S. Kim, *Sci. Rep.* **2020**, *10*, 14194.
- [98] Y. Wang, Y. Zhang, C. Tang, J. Yu, H. He, H. Qi, *Tribol. Int.* **2020**, *144*, 106128.
- [99] D. Sun, K. F. Böhringer, *Appl. Phys. Lett.* **2020**, *116*, 093702.
- [100] H. Shirinkami, J. Kim, C. Lee, H. C. Kim, H. Chun, *BioChip J.* **2017**, *11*, 316.
- [101] J. Li, C. J. Kim, *Lab Chip* **2020**, *20*, 1705.
- [102] C. Li, H. Jjiang, *Micromachines* **2014**, *5*, 432.
- [103] D. Kopp, T. Brender, H. Zappe, *Appl. Opt.* **2017**, *56*, 3758.
- [104] X. Song, H. Zhang, D. Li, D. Jia, T. Liu, *Sci. Rep.* **2020**, *10*, 16318.
- [105] I. S. Park, Y. Park, S. H. Oh, J. W. Yang, S. K. Chung, *Sens. Actuators, A* **2018**, *273*, 317.
- [106] W. C. Nelson, C.-J. Å. C. Kim, *J. Adhes. Sci. Technol.* **2012**, *26*, 1747.
- [107] H. T. Li, Y. H. Huang, D. J. Yao, *Proc. IEEE Int. Conf. Micro Electro Mech. Syst.*, Belfast, Ireland **2018**, p. 1138.
- [108] E. Samiei, M. Hoorfar, *Miniature Fluidic Devices for Rapid Biological Detection*, **2018**, pp. 171–205.
- [109] K. Ugsornrat, T. Maturros, P. Pasakon, C. Karuwan, T. Pogfay, C. Sriprachuabwong, A. Wisitsoraat, A. Tuantranont, *Mater. Sci. Eng., B* **2018**, *238–239*, 36.
- [110] X. Rui, S. Song, W. Wang, J. Zhou, *Biomicrofluidics* **2020**, *14*, 061503.
- [111] A. B. Alias, C.-E. Chiang, H.-Y. Huang, K.-T. Lin, P.-J. Lu, Y.-W. Wang, T.-H. Wu, P.-S. Jjiang, C.-A. Chen, D.-J. Yao, *Sci. Rep.* **2020**, *10*, 9708.
- [112] M.-S. Lee, W. Hsu, H.-Y. Huang, H.-Y. Tseng, C.-T. Lee, C.-Y. Hsu, Y.-C. Shieh, S.-H. Wang, D.-J. Yao, C.-H. Liu, *Biosens. Bioelectron.* **2020**, *150*, 111851.
- [113] H. Lee, S. Lee, I. Jang, J. Kim, G. You, E. Kim, K. Choi, J. H. Lee, S. Choi, K. Shin, M.-H. Yoon, H. B. Oh, *Microfluid. Nanofluid.* **2017**, *21*, 141.
- [114] J. Wang, P. H. Chao, S. Hanet, R. M. Van Dam, *Lab Chip* **2017**, *17*, 4342.
- [115] V. Jain, K. Muralidhar, *Trans. Indian Natl. Acad. Eng.* **2020**, *5*, 251.
- [116] S. Petralia, D. Motta, S. Conoci, *Biotechnol. Bioeng.* **2019**, *116*, 2087.
- [117] A. R. Wheeler, H. Moon, C.-J. Å. C. Kim, J. A. Loo, R. L. Garrell, *Anal. Chem.* **2004**, *76*, 4833.
- [118] X. Min, C. Bao, W. S. Kim, *ACS Sens.* **2019**, *4*, 918.
- [119] L. Malic, T. Veres, M. Tabrizian, *Biosens. Bioelectron.* **2009**, *24*, 2218.
- [120] G. S. Bindiganavale, M. Amaya, H. Moon, *J. Micromech. Microeng.* **2018**, *28*, 125015.
- [121] Z. Yan, M. Jin, Z. Li, G. Zhou, L. Shui, *Micromachines* **2019**, *10*, 89.
- [122] G. Bindiganavale, S. You, H. Moon, *Proc. IEEE Int. Conf. Micro Electro Mech. Syst.*, **2014**, pp. 1039–1042.
- [123] S.-Y. Park, Y. Nam, *Micromachines* **2017**, *8*, 3.
- [124] R. Yan, et al., *Appl. Phys. Lett.* **2018**, *112*, 243701.



Oriol Caro-Pérez graduated in biomedical sciences at Barcelona University. Then he obtained Masters degrees in molecular biotechnology (University of Barcelona) and statistics and bioinformatics (Open University of Catalonia) in 2018 and 2019, respectively. After finishing his training and a brief period in a bioinformatics company, Oriol joined the Microtech and Celbiotech groups of the UPC as a doctoral student, where he develops a paper-based device for immediate biodiagnosis.



Jasmina Casals-Terré received the M.S. degree in mechanical and aerospace engineering from the University of California, Irvine, in 2002 and in 2007 a Ph.D. in design, fabrication, and testing of bistable micro-electro-mechanica-systems (MEMS) switches. She joined the Faculty of UPC-BarcelonaTech in 2007 and became a full professor in 2020 in the Department of Mechanical Engineering. She established the Microfluidics Research Group in UPC, where her research interests focus on radio-frequency micro-electro-mechanica-systems (RF MEMS), biomicrofluidics for medical diagnosis and optimized tribology. She has more than ten years of experience in research project management (leading several european, national, and regional projects) and she has authored more than 30 peer-reviewed papers (most of them in Q1).



M. Blanca Roncero is an associate professor of paper engineering in the School of Industrial, Aerospace and Audiovisual Engineering of Terrassa (Spain). She is also leading the CELBIOTECH research group. She received her degree in industrial engineering in 1995 and the Ph.D. degree in textile and paper engineering in 2001, from the Polytechnic University of Catalonia. Her research is focused on the utilization of lignocellulosic materials in novel and multifunctional applications. Her recent efforts deal with the chemical and biotechnological functionalization of cellulose to obtain laminar structures with new and advanced properties to be used in biopackaging and biosensing.